Glucose-regulated *O*-GlcNAcylation of DNMT1 inhibits DNA methyltransferase activity and maintenance of genomic methylation

Heon Shin[a], Amy Leung[a], Kevin R. Costello[a,b], Parijat Senapati[a], Hiroyuki Kato[a], and Dustin E. Schones[a,b,1]

[a]Department of Diabetes Complications and Metabolism, Beckman Research Institute, City of Hope, Duarte, California 91010 USA; [b]Irell and Manella Graduate School of Biological Sciences, City of Hope, Duarte, California 91010 USA

Author Contributions: H.S., A.L., and D.E.S. designed research; H.S., A.L., and H.K. performed research; H.S., A.L., K.C., and P.S. analyzed data; and H.S., A.L., and D.E.S. wrote the paper.

Competing Interest Statement: The authors declare no competing interest.

Classification: Biological Sciences; Biochemistry

Data deposition: Data are available in the Gene Expression Omnibus (GEO) database (accession no. GSE201470)

[1]To whom correspondence may be addressed. Email: dschones@coh.org

Keywords: *O*-GlcNAcylation, Epigenetics, Metabolism

This PDF file includes:
Main Text
Figures 1 to 4

Abstract

The production of *O*-GlcNAc for protein *O*-GlcNAcylation is highly tuned to the metabolic state of the cell and thus can serve as a nutrient sensor responding to changes in metabolic pathways. We report here that excess glucose leads to increased *O*-GlcNAcylation of DNMT1, resulting in inhibition of DNA methyltransferase 1 (DNMT1) function and alterations to the epigenome. Using mass spectrometry and complementary alanine mutation experiments, we identified S878 as the major residue that is *O*-GlcNAcylated on DNMT1. Functional studies reveal that *O*-GlcNAcylation of DNMT1-S878 reduces its DNA methyltransferase activity. Treatment of cells with prolonged high glucose induces loss of DNA methylation, preferentially at partially methylated domains (PMDs). These results establish *O*-GlcNAcylation of DNMT1 as a mechanism through which the epigenome is regulated by glucose metabolism and implicates a role for glycosylation of DNMT1 in metabolic diseases characterized by hyperglycemia.

Significance

Glucose metabolism results in production of *O*-GlcNAc, the substrate for protein *O*-GlcNAcylation. The posttranslational modification of proteins with *O*-GlcNAcylation thereby serves as a nutrient sensor. We report that excess glucose leads to increased *O*-GlcNAcylation of DNMT1, resulting in inhibition of DNA methyltransferase 1 (DNMT1) function. We furthermore show that inhibition of DNMT1 function through increased *O*-GlcNAcylation results in loss of DNA methylation, preferentially at partially methylated domains (PMDs).

Introduction

Excess glucose, or hyperglycemia, is a hallmark of obesity and the defining clinical feature of diabetes (1). Metabolically, hyperglycemia leads to cellular glucose uptake which, in turn, increases flux of glucose utilization pathways and production of metabolites (2). One downstream

output of glucose metabolism is the nucleotide sugar, UDP-GlcNAc, that is used as a substrate for protein *O*-GlcNAcylation (2, 3).

Protein *O*-GlcNAcylation is a dynamic and reversible post-translational modification that attaches a single *O*-linked β-*N*-acetylglucosamine to serine or threonine residues (4). It is modulated by two *O*-GlcNAc cycling enzymes, *O*-GlcNAc transferase (OGT) and *O*-GlcNAcase (OGA) depending on nutritional status (3, 5). The increased concentration of UDP-GlcNAc that is observed in conditions of excess glucose leads to increased protein *O*-GlcNAcylation (6). Obesogenic diets have been shown to have elevated protein *O*-GlcNAcylation in various human cell types, including the liver (7), lymphocytes (8), and immune cells (9).

As with other post-translational modifications, *O*-GlcNAcylation of proteins can influence the function and/or stability of the targeted proteins (10, 11). Thousands of proteins are targets for *O*-GlcNAcylation, including many epigenetic regulatory proteins. For example, the *O*-GlcNAcylation of TET family proteins impacts their activity, localization and targeting (12-15). All DNA methyltransferases have furthermore been shown to be *O*-GlcNAcylated, although the functional consequences of this are unclear (16).

Among the DNA methyltransferase (DNMT) family of proteins, DNMT1 is imperative for maintaining DNA methylation patterns in replication (17). DNMT1 is a modular protein with several domains necessary for interacting with cofactors, including the BAH1 and BAH2 domains (18, 19). The stability and function of DNMT1 has been shown to be regulated through post-translational modifications including acetylation, phosphorylation, and methylation (20).

Partially methylated domains, large domains with a loss of DNA methylation, were originally identified in cultured cell lines (21) and subsequently found to be a characteristic of cancer cells (22, 23). PMDs have also been detected in non-cancerous healthy tissues, where they are associated with late replication loci (24, 25). While PMDs are generally thought to arise from a lack of fidelity in maintenance methylation (26), the mechanisms responsible for the establishment of PMDs have remained unclear. Here, we report that the activity of DNMT1 is

regulated by extracellular levels of glucose through its *O*-GlcNAcylation resulting in loss of methylation at PMDs.

Results

High glucose conditions increase *O*-GlcNAcylation of DNMT1

To validate that DNMT1 can be *O*-GlcNAcylated, we treated Hep3B cells with OSMI-4 (OSMI), an OGT inhibitor (27), as well as with Thiamet-G (TMG), an OGA inhibitor (28). As expected, immunoblots of cellular lysate with an antibody recognizing pan-*O*-GlcNAc (RL2) reveal that inhibition of OGA increased global levels of *O*-GlcNAc while inhibition of OGT decreased global levels of *O*-GlcNAc (*SI Appendix,* Fig. S1 *A*). To distinguish whether DNMT1 is *O*-GlcNAcylated, immunoprecipitates from the cellular lysates treated with OSMI or TMG were generated with DNMT1 antibodies. Immunoblots with *O*-GlcNAc antibodies reveal that TMG treatment increases *O*-GlcNAc of DNMT1 while OSMI treatment decreases *O*-GlcNAc (*SI Appendix,* Fig. S1 *B*). In addition to Hep3B cells, we found that DNMT1 is *O*-GlcNAcylated in HepG2 cells and B cell derived lymphocytes, indicating DNMT1 is *O*-GlcNAcylated across various cell types (*SI Appendix,* Fig. S1 *C* and *D*).

To assess the effect of increased glucose metabolism on *O*-GlcNAcylation of DNMT1, we treated Hep3B cells with glucose or sucrose (5mM or 25mM) and examined global protein *O*-GlcNAcylation as well as the *O*-GlcNAcylation of DNMT1 specifically. Consistent with previous reports (29), the total amount of protein *O*-GlcNAcylation was increased with 25mM of glucose (Fig. 1*A*). Global protein *O*-GlcNAcylation was also induced with 25mM sucrose, albeit to a lower extent than with glucose (Fig. 1*A*). To specifically assess the level of *O*-GlcNAcylated DNMT1, we performed immunoprecipitation of DNMT1 from lysates of glucose treated Hep3B cells and immunoblotted for *O*-GlcNAc. As with the analysis of total protein, high glucose treatment (25mM) increased the expression of *O*-GlcNAcylation of DNMT1 (Fig. 1 *B* and *SI Appendix,* S1 *E*). To examine whether an increase of *O*-GlcNAcylation of DNMT1 also occurs in primary cells, we

collected peripheral blood mononuclear cells (PBMCs) from three separate donors and treated the PBMCs with increasing glucose levels (0mM, 5mM, 10mM, 15mM, and 20mM). Similar to our observations in Hep3B cells, we observed an increase in *O*-GlcNAcylation of DNMT1 with increased glucose (Fig. 1 *C* and *D*). These data validate the *O*-GlcNAcylation of DNMT1 and that the degree of modification of DNMT1 increases with glucose concentrations.

Identification of the major *O*-GlcNAcylation sites of DNMT1

To begin to identify the major residues *O*-GlcNAcylated on DNMT1 we utilized OGTsite (http://csb.cse.yzu.edu.tw/OGTSite/index.php) (30) to predict potential sites of *O*-GlcNAcylation. OGTsite, which uses experimentally verified *O*-GlcNAcylation sites to build models of substrate motifs, identified 22 candidate *O*-GlcNAc modified sites on human DNMT1 (*SI Appendix,* Table S1). We next employed mass spectrometry analysis to examine the post-translational modifications on DMNT1 in Hep3B cells. We generated a construct with Myc-tagged DNMT1 to increase the level of expressed DNMT1. Immunoblots with Myc antibody (31) revealed a band corresponding to Myc-DNMT1 in transfected, but not mock transfected, cells (*SI Appendix,* Fig. S2 *A*). We further confirmed with immunoprecipitation followed by immunoblot that the overexpressed Myc-DNMT1 can be *O*-GlcNAcylated (*SI Appendix,* Fig. S2 *B*). For mass spectrometry analysis, we treated Myc-DNMT1 expressing cells with 25mM Thiamet-G (TMG) to further increase the *O*-GlcNAcylation of DNMT1. Myc-DNMT1 was enriched from transfected cells by monoclonal Ab-crosslinked immunoprecipitation and subjected to in-solution digestion using three different enzymes (AspN, chymotrypsin, and LysC) and high-resolution LC-MS/MS analysis. Peptide analyses revealed that S878, which is located on the bromo-associated homology (BAH1) domain of the DNMT1 is *O*-GlcNAcylated (Fig. 2 *A* and *B* and *SI Appendix,* S2 *C*; Table S2). In addition, eight unreported phosphorylated residues were newly detected (T208, S209, S873, S874, S953, S954, S1005, and S1202) (*SI Appendix,* Table S2).

We chose the three top candidates based on prediction score (T158, T616, and T882) as well as the site identified from mass spectrometry analysis (S878) for further analysis with alanine mutation experiments. The threonine/serine residues were mutated to alanine residues on our Myc-DNMT1 construct and *O*-GlcNAcylation was evaluated with immunoblot following immunoprecipitation. Loss of threonine and serine at positions T158 and S878 respectively resulted in a loss of *O*-GlcNAcylation, indicating that these two residues are required for *O*-GlcNAcylation, with the DNMT1-S878A mutant resulting in > 50% reduction of *O*-GlcNAcylation (Fig. 2 *C*). These results indicate that T158 (near the PCNA binding domain) and S878 (within the BAH1 domain) are the DNMT1 residues modified with *O*-GlcNAcylation.

_O_-GlcNAcylation of DNMT1 results in loss of DNA methyltransferase activity

The BAH domains of DNMT1 have been found to be necessary for DNA methyltransferase activity (32). Given that S878 is in the BAH1 domain, we reasoned that *O*-GlcNAcylation of this residue could impact the DNA methyltransferase activity of DNMT1. To test this, we treated Hep3B cells with either 5mM or 25mM of glucose as well as with 25 mM Thiamet-G (TMG) or DMSO as control and evaluated the DNA methyltransferase activity of immunoprecipitated DNMT1 with the EpiQuik DNMT Activity/Inhibition ELISA Easy Kit (EpiGentek, details in STAR Methods). Intriguingly, high glucose (25mM) treatment reduced the activity of DNMT1 and additional treatment of cells with TMG further inhibited the activity of DNMT1 (Fig. 3 *A* and *SI Appendix,* S3 *A*).

To examine whether elevated glucose affected the function of DNMT1 in primary cells, we treated PBMCs with increasing concentrations of glucose (0mM, 5mM, 10mM, 15mM, 20mM and 25mM with Thiamet-G) for 96 hours and analyzed the DNA methyltransferase activity of DNMT1. We observed a striking dose-dependent inhibition of the DNA methyltransferase activity of DNMT1 (Fig. 3 *B* and *C*). Together, these data indicate that elevated levels of extracellular glucose can inhibit the methyltransferase function of DNMT1.

We next examined the ability of the DNMT1 alanine mutants (DNMT1-T158A and DNMT1-S878A) to attenuate the impact of high glucose- and TMG-induced loss of DNA methyltransferase activity. Compared to the DNA methyltransferase activity of DNMT1-WT (Myc-DNMT1-WT), which is sensitive to high glucose/TMG treatment, the DNA methyltransferase activity of Myc-DNMT1-S878A is not inhibited by high glucose treatment (Fig. 3 *D*). In contrast, the DNA methyltransferase activity of Myc-DNMT1-T158A is inhibited by high glucose/TMG treatment in a manner similar to DNMT1-WT, indicating that *O*-GlcNAcylation of DNMT1-T158 does not affect its DNA methyltransferase activity.

A previous phosphoproteomic analysis revealed that DNMT1-S878 can be phosphorylated (33). To evaluate the potential that phosphorylation, rather than *O*-GlcNAcylation, of S878 is leading to the loss of DNA methyltransferase activity, we generated Myc-DNMT1-S878D, a phosphomimetic mutant that cannot be *O*-GlcNAcylated, and examined DNA methyltransferase activity in normal and high glucose conditions. This phosphomimetic mutant did not have loss of DNA methyltransferase activity under high glucose conditions, indicating that *O*-GlcNAcylation of S878 but not phosphorylation of S878 is leading to loss of methyltransferase activity of DNMT1 (Fig. 3 *D*).

_O_-GlcNAcylation of DNMT1 results in subsequent loss of DNA methylation

Given our observations that *O*-GlcNAcylation of DNMT1 under high glucose/TMG inhibits its DNA methyltransferase activity, we reasoned that these conditions would result in a general loss of DNA methylation. To assess this, DNA methylation was assayed using the global DNA methylation LINE-1 kit (Active Motif, details in STAR Methods) as a proxy for global methylation. Comparison of DNA methylation levels under high glucose and TMG with a DNA methylation inhibitor (5-aza; details in STAR Methods) revealed that high glucose leads to a loss of DNA methylation in a manner comparable with the DNA methylation inhibitor (Fig. 3 *E*). This methylation loss was not apparent in the Myc-DNMT1-S878A mutant, further demonstrating that

O-GlcNAcylation of S878 serine within DNMT1 directly affects DNA methylation under high glucose conditions (Fig 3 *E* and *SI Appendix,* Fig. S3 *B*). A complementary assessment of DNA methylation using methylation sensitive restriction enzymes and gel electrophoresis (details in STAR Methods) revealed similar trends (*SI Appendix,* Fig S3 *C*).

_O_-GlcNAcylation of DNMT1 results in loss of DNA methylation at partially methylated domains (PMDs)

To further examine alterations to DNA methylation upon high glucose induced *O*-GlcNAcylation of DNMT1, we performed genomic methylation profiling with nanopore sequencing (ONT PromethION; details in STAR Methods). The Myc-DNMT1 overexpressed cell lines (Myc-DNMT1-WT and Myc-DNMT1-S878A) were treated with TMG and either 5mM or 25mM glucose and DNA methylation was profiled in duplicate. Considering only CpGs with > 5x coverage (*SI Appendix,* Fig. S4 *A*), we observed a global loss of methylation in the high glucose/TMG treatment compared to control (Fig. 4 *A* and *B* and *SI Appendix,* S4 *B*-*G*). Conversely, for the DNMT1-S878A mutant, there was no appreciable decrease in DNA methylation by high glucose/TMG treatment (Fig. 4 *A*). These results collectively indicate that *O*-GlcNAcylation of S878 of DNMT1 leads to a global loss of DNA methylation.

Examination of DNA methylation changes induced by *O*-GlcNAcylation of DNMT1 revealed a preferential loss of DNA methylation at liver cancer PMDs (34) that was not observed in S878A mutant cells (Fig. 4 *B* and *C*). Partially methylated domains (PMDs) have several defining features, including being relatively gene poor and harboring mostly lowly transcribed genes (26). We stratified the genome in terms of gene density and transcription rate (see STAR Methods for details) and found that regions that lose methylation in high glucose conditions are largely gene poor (Fig. 4 *D*) and contain lowly transcribed genes (*SI Appendix,* Fig. S4 *H*) (35). PMDs have furthermore been linked to regions of late replication associated with the nuclear lamina (23). We therefore examined the correlation between loss of methylation caused by high

glucose/TMG and replication timing (36). In DNMT1-WT cells, late replication domains preferentially lose DNA methylation in high glucose/TMG conditions compared to early replication domains (Fig. 4 *E*). This loss of methylation was not observed in S878A mutant cells (*SI Appendix,* Fig. S4 *I*).

It has previously been demonstrated that certain genes within PMDs "escapee" the general loss of methylation and reduced expression observed in PMDs (26). We found 270 genes within PMDs that retained methylation and transcription signatures in high glucose conditions, including 147 that overlap with other cell types (26) (*SI Appendix,* Fig. S4 *J*).

One of the major functions of DNA methylation in mammalian genomes is the repression of repetitive elements (37). It has furthermore been shown that many chromatin proteins involved in the repression of transposable elements (TEs) are capable of being *O*-GlcNAcylated (16). We therefore examined the potential of *O*-GlcNAcylation of DNMT1 to lead to loss of suppression of TEs. We found that high glucose conditions resulted in methylation loss at TEs in a manner similar to the non-repetitive fraction of the genome (*SI Appendix,* Fig. S5 *A*), with a more dramatic loss of methylation at LINEs and LTRs as compared to SINE elements (*SI Appendix,* Fig. S5 *B-D*). Given that evolutionarily recent TEs are more likely to lose methylation than older elements in a variety of systems (38, 39), we examined the methylation status of two younger subfamilies, LTR12C (*Hominoidea*) and HERVH-int (*Catarrhini*) elements (*SI Appendix,* Fig. S5 *E*). While HERVH-int elements show a loss of methylation similar to the rest of the genome, LTR12C elements do not lose methylation in the same manner (*SI Appendix,* Fig. S5 *E* and *F*) suggesting they are protected from the loss of methylation. Stratifying all TEs by evolutionary age and examining the methylation changes induced by *O*-GlcNAcylation of DNMT1 for each clade revealed that evolutionarily recent elements are less likely to lose methylation (*SI Appendix,* Fig. S5 *G*).

Discussion

Although there is a great deal of evidence regarding the important regulatory role of *O*-GlcNAcylation in gene regulation (40), a direct link with DNA methylation has not previously been established. The maintenance methyltransferase DNMT1 is essential for faithful maintenance of genomic methylation patterns and mutations in DNMT1, particularly in the BAH domains, lead to disruption of DNA methylation (32). While it has been shown that DNTM1 can be *O*-GlcNAcylated (16), the site of *O*-GlcNAc modification on DNMT1 as well as the functional consequences of this modification have not previously been examined.

We reveal that *O*-GlcNAcylation of DNMT1 impacts its DNA methyltransferase activity and affects DNMT1 function leading to loss of DNA methylation at PMDs. PMDs are observed in both healthy and cancerous cells and have been suggested to be associated with mitotic dysfunction. However, models for how these domains are established remain incomplete (26). The results presented here suggest an additional layer whereby *O*-GlcNAcylation of DNMT1 at S878 due to increased glucose levels can inhibit the function of DNA methyltransferase activity of DNMT1, resulting in loss of methylation and establishment of partially methylated domains.

Metabolic diseases such as obesity and diabetes have been linked to epigenetic changes that alter gene regulation (41). It has previously been established that there is a general increase in protein *O*-GlcNAcylation in hyperglycemia conditions (42) and several epigenetic regulatory factors have been shown to have increased *O*-GlcNAcylation under high glucose conditions (43-45). Our findings that extracellular glucose promotes *O*-GlcNAcylation of DNMT1 and inhibition of DNMT1's function in maintenance of genomic methylation provide direct evidence that extracellular levels of glucose is linked with epigenomic regulation.

Materials and Methods

Cell culture and plasmid DNA transfection. Hepatocellular carcinoma cell lines (HepG2, and Hep3B) were purchased from ATCC (Manassas, VA, USA). All cell lines were shown to be negative in mycoplasma test using MycoScope (MY01050, Genlantis, San Diego, CA, USA). The

following ATCC-specified cell culture media were used: Dulbecco's modified Eagle's medium (DMEM, 11885-084, Grand Island, NY, USA) or high glucose Dulbecco's modified Eagle's medium (DMEM, 11995-065, Gibco, Grand Island, NY, USA) with 10% fetal bovine serum (FBS, SH30910.03, HyClone, South Logan, UT, USA) and Opti-MEM (1869048, Gibco, Grand Island, NY, USA). All cells were cultured in a 37°C with a 5% CO_2 atmosphere incubator. HepG2 and Hep3B cells were transiently transfected (with the pcDNA3 with or without DNMT1 cDNA) using Lipofectamine 3000 (Invitrogen, Carlsbad, CA, USA) and selected with Geneticin (G418, 10131-035, Gibco, Grand Island, NY, USA) according to the manufacturer's instructions. Human DNMT1 plasmid was purchased from Addgene (Watertown, MA, USA).

Isolation of peripheral blood mononuclear cells (PBMCs). PBMCs such as lymphocyte, monocyte or a macrophage were isolated directly from whole blood using Ficoll-Paque (Premium, GE Healthcare, Chicago, IL, USA) density gradient centrifugation. 15ml whole blood was mixed with same volume of phosphate-buffered saline containing 0.1% Fetal bovine serum + 2mM EDTA (PBS solution). Next, the blood mix was placed on top of 15 ml Ficoll and centrifuged at 400g to 200g for 40 min without brake. Next, remove the supernatant and washed three times with PBS solution.

Isolation of B cells and Epstein-Barr virus (EBV) infection for lymphocyte transformation. $CD19^+$ B cells were isolated from PBMCs (peripheral blood mononuclear cells) using Dynabeads $CD19^+$ pan B (11143D, Invitrogen, Carlsbad, CA, USA) according to the manufacturer's instruction. 2.5 x 10^8 cells of PBMCs were resuspended in 10ml Isolation buffer (PBS, 0.1% BSA, 2mM EDTA). 250 µl of pre-washed beads were added to PBMCs and incubated for 20 min in 4°C with gentle rotation. For positive isolation of $CD19^+$ B cells, beads and supernatant were separated using magnet, and supernatant was discarded. Beads were washed three times, and beads bounded with $CD19^+$ B cells were resuspended with 2.5 ml of cell culture medium (80%

RPMI1640, 20 % heat-inactivated FBS, Glutamine). $CD19^+$ B cells were released from Dynabeads using DETACHaBEAD (Invitrogen, ca12506D) according to the manufacturer's instruction.

B cells were infected with Epstein-Barr virus (EBV) to transform lymphocyte. 10 ml of B cells were transferred into T75 flask. 1.5ml of stock EBV collected from a B95-8 strain-containing marmoset cell lines and 1ml of Phytohemagglutinin P (PHA-P) were added to flask and incubated in a 37°C with a 5% CO_2 atmosphere incubator. Every 5 to 7 days, 10 ml of cell culture medium was added. Cells were let to grow in CO_2 atmosphere incubator for 30 days until all B cells were transformed to LCL.

Immunoprecipitation and western blot analysis. Cell lysates were incubated with specific antibodies and lysis buffer for 4 hours. Subsequently, 30 µl of washed Dynabeads (14311D, Thermo Fisher, Waltham, MA, USA) were added to each lysate and incubated overnight at 4°C. Next, the beads were washed five times, and the antigens were eluted twice using 8M Urea buffer (8M Urea, 20mM Tris pH 7.5, and 100mM NaCl) and concentrated. The resulting samples were separated by Mini-PROTEAN TGX (4-20%, 4561093, Bio-Rad Laboratories, Hercules, CA, USA) and transferred onto nitrocellulose membranes (Amersham Hybond, 10600021, GE Healthcare, Chicago, IL, USA) using Trans-Blot SD Semi-dry Transfer Cell system (Bio-Rad Laboratories, Hercules, CA, USA). The membranes were then blocked with 5% skim milk in Tris-buffered saline + Tween-20 (TBS-T; 20 mM Tris, 137 mM NaCl, 0.1% Tween-20, pH 7.6), incubated overnight at 4°C with a 1:1000 dilution of each antibodies, and subsequently incubated for 1 h with a 1:5000 dilution of a horseradish peroxidase–conjugated goat anti-mouse secondary antibody (ab6789, Abcam, Cambridge, UK) or goat anti-rabbit secondary antibody (ab6721, Abcam, Cambridge, UK). Immunoreactive proteins were detected using SuperSignal West Dura Extended Duration Substrate (34076, Thermo, Rockford, IL, USA) and detected using a ChemiDoc MP Imaging

system (Bio-Rad Laboratories, Hercules, CA, USA). The band intensity was densitometrically evaluated using Image Lab software (Version 5.2, Bio-Rad Laboratories, Hercules, CA, USA).

Protein identification using the Thermo Fusion Lumos system LC-MS/MS. LC-MS separation was performed on an Thermo Fusion Lumos system (Thermo Scientific, Waltham, MA, USA). For LC separation, 60-minute LC gradient on EasySpray column (particle sizes: 500 mm, 75 μm) was used for peptide separation. Mass spectra for peptide identification or quantification were acquired using an Orbitrap Lumos mass at 120,000 resolutions. Full MS scan ranges were acquired from 156 to 2000 m/z. MS/MS spectra were acquired at a resolution of 30,000 using HCD at 35% collision energy.

Identify post-translational modifications on DNMT1 using complementary in-solution digestion with three enzymes (chymotrypsin, AspN and LysC). Protein was reduced with DTT and alkylated with iodoacetamide. Aliquots of protein were separately digested with three enzymes and peptides were desalted using a C18 tip.

Raw data files were submitted to Byonic (v2.16.11) for target decoy search against the human protein database (uniprot/swissprot, 2020). Peptide-level confidence threshold was set at 99% (FDR <0.01). The sample was bracketed by *E. coli* QC runs, which were then correlated to ensure instrument quality. QC passed threshold (≥ 0.9) with an R^2 of 0.98 (correlation value, R=0.99)

Site-directed point mutation. Specific primers for serine (S) and threonine (T) to alanine (A) and aspartic acid (D) mutations of DNMT1 were designed and used to site-directed point mutations in a plasmid vector. A PCR-amplified DNA fragment of pcDNA3-DNMT1 was generated using Q5 Site-Directed Mutagenesis Kit (E0554S, NEB, Ipswich, MA, USA). The primers used in this process are described in Supporting Information. After PCR, the non-mutated sequences were cleaved using Q5 KLD enzyme (NEB) according to the manufacturer's instructions. The mutated

vectors were transformed into E. coli competent cells that were cultured and prepared using a GenElute HP Plasmid Midi kit (NA0200-1KT, Sigma-Aldrich, St. Louis, MO).

DNA methyltransferase activity assay. DNA methyltransferase activities of endogenous DNMT1 and recombinant DNMT1 were measured by EpiQuik DNMT Activity/Inhibition ELISA Easy Kit (P-3139-48, EpiGentek, Farmingdale, NY, USA) according to the manufacturer's instructions. The endogenous DNMT1 (by anti-DNMT1 Ab, 60B1220.1) and recombinant DNMT1 (by anti-Myc, ab18185) were enriched using immunoprecipitation from each cell or tissue lysates. DNMT1s were isolated and normalized by BCA analysis. The activity of 5 ng DNMT1 was analyzed by 450nm ELISA with an optimal wavelength of 655nm.

Global DNA Methylation LINE-1 assay. Global DNA methylation LINE-1 were measured by Active Motif (55017, Carlsbad, CA, USA) according to the manufacturer's instructions. Each Hep3B and myc-DNMT1 overexpressed mutants (DNMT1-WT or DNMT1-S878A) were treated 5mM glucose, or 25mM glucose, and 5-aza (negative control). The activity of 100 ng was analyzed by 450nm ELISA with an optimal wavelength of 655nm.

Agilent 4200 TapeStation. Global DNA methylation were measured by Agilent 4200 TapeStation system (Santa Clara, CA, USA) with the Genomic DNA ScreenTape (5064-5365) and Genomic DNA Reagent (5067-5366) according to the manufacturer's instructions.

Nanopore PromethION sequencing. Reads were aligned using minimap2 (RRID:SCR_018550) with the options -a -x map-ont (46). Methylation state of CpGs was called using nanopolish (RRID:SCR_016157) with the options call-methylation -t 100 (47). Only loci with greater than 5 x coverage were considered in the analysis. Methylation percentage was averaged across CpG islands.

RNA sequencing data. Hep3B RNA-seq data were obtained from a previous publication (35). Fastq files were aligned using HISAT2 version 2.1.0 (RRID:SCR_015530) to the hg19 genome. Duplications are removed using picard version 2.10.1 (RRID:SCR_006525). Aligned reads were sorted using samtools version 1.10 (RRID:SCR_002105). UCSC genome browser tracks were established using bedGraphToBigWig. FPKM was calculated using StringTie version 1.3.4d (RRID:SCR_016323).

For all datasets, Bedgraph files were generated using bedtools version 2.29.0 (RRID:SCR_006646). BigWigs were generated using the UCSCtools bedGraphToBigWig. Heatmap of global DNA methylation for DNMT1-WT and DNMT1-S878A cells under low or high glucose were generated using a custom script to profile the read coverage at each base and were visualized using pheatmap version 1.0.12 (RRID:SCR_016418). All other heatmaps and aggregate plots of loci that extend were generated using deeptools (RRID:SCR_016366).

Statistical Analysis. Statistical analyses were performed and graphed using Graphpad Prism 9 (v9.3.1). All statistical tests were performed by three independent experiments assay, and the data are presented as means ± standard deviations. *$p < 0.001$; **$p < 0.0005$; ***$p < 0.0001$ by Student's *t*-test (A and B); n.s., not significant; Data are represented as mean ± SD.

Data availability. PromethION sequencing data have been deposited in the NCBI Gene Expression Omnibus (GEO) under accession no. GSE201470.

ACKNOWLEDGEMENTS. This manuscript is dedicated to the memory of Dr. Arthur Riggs. This work was supported by the National Institutes of Health, grants R01DK112041 and R01CA220693 (D.E.S.). Research reported in this publication included work performed in the Pathology and Integrative Genomics Cores of the City of Hope and was supported by the City of Hope CCSG

Pilot award from National Cancer Institute of the National Institutes of Health under award number P30CA033572.

References

1. American Diabetes Association, Diagnosis and classification of diabetes mellitus. *Diabetes care* **32 Suppl 1**, S62-67 (2009).
2. M. Hawkins, I. Angelov, R. Liu, N. Barzilai, L. Rossetti, The tissue concentration of UDP-N-acetylglucosamine modulates the stimulatory effect of insulin on skeletal muscle glucose uptake. *The Journal of biological chemistry* **272**, 4889-4895 (1997).
3. C. Slawson, R. J. Copeland, G. W. Hart, O-GlcNAc signaling: a metabolic link between diabetes and cancer? *Trends in biochemical sciences* **35**, 547-555 (2010).
4. G. W. Hart *et al.*, O-GlcNAcylation of key nuclear and cytoskeletal proteins: reciprocity with O-phosphorylation and putative roles in protein multimerization. *Glycobiology* **6**, 711-716 (1996).
5. G. W. Hart, M. P. Housley, C. Slawson, Cycling of O-linked beta-N-acetylglucosamine on nucleocytoplasmic proteins. *Nature* **446**, 1017-1022 (2007).
6. J. L. Walgren, T. S. Vincent, K. L. Schey, M. G. Buse, High glucose and insulin promote O-GlcNAc modification of proteins, including alpha-tubulin. *Am J Physiol Endocrinol Metab* **284**, E424-434 (2003).
7. C. Guinez *et al.*, O-GlcNAcylation increases ChREBP protein content and transcriptional activity in the liver. *Diabetes* **60**, 1399-1413 (2011).
8. C. R. Torres, G. W. Hart, Topography and polypeptide distribution of terminal N-acetylglucosamine residues on the surfaces of intact lymphocytes. Evidence for O-linked GlcNAc. *The Journal of biological chemistry* **259**, 3308-3317 (1984).
9. T. de Jesus, S. Shukla, P. Ramakrishnan, Too sweet to resist: Control of immune cell function by O-GlcNAcylation. *Cell Immunol* **333**, 85-92 (2018).
10. X. Yang, K. Qian, Protein O-GlcNAcylation: emerging mechanisms and functions. *Nature reviews. Molecular cell biology* **18**, 452-465 (2017).
11. H. Shin *et al.*, O-GlcNAcylation of the Tumor Suppressor FOXO3 Triggers Aberrant Cancer Cell Growth. *Cancer Res* **78**, 1214-1224 (2018).
12. Q. Chen, Y. Chen, C. Bian, R. Fujiki, X. Yu, TET2 promotes histone O-GlcNAcylation during gene transcription. *Nature* **493**, 561-564 (2013).
13. R. Ito *et al.*, TET3-OGT interaction increases the stability and the presence of OGT in chromatin. *Genes Cells* **19**, 52-65 (2014).
14. F. T. Shi *et al.*, Ten-eleven translocation 1 (Tet1) is regulated by O-linked N-acetylglucosamine transferase (Ogt) for target gene repression in mouse embryonic stem cells. *The Journal of biological chemistry* **288**, 20776-20784 (2013).
15. Q. Zhang *et al.*, Differential regulation of the ten-eleven translocation (TET) family of dioxygenases by O-linked beta-N-acetylglucosamine transferase (OGT). *The Journal of biological chemistry* **289**, 5986-5996 (2014).

16. M. Boulard, S. Rucli, J. R. Edwards, T. H. Bestor, Methylation-directed glycosylation of chromatin factors represses retrotransposon promoters. *Proceedings of the National Academy of Sciences of the United States of America* **117**, 14292-14298 (2020).
17. T. H. Bestor, V. M. Ingram, Two DNA methyltransferases from murine erythroleukemia cells: purification, sequence specificity, and mode of interaction with DNA. *Proc Natl Acad Sci U S A* **80**, 5559-5563 (1983).
18. W. Ren, L. Gao, J. Song, Structural Basis of DNMT1 and DNMT3A-Mediated DNA Methylation. *Genes (Basel)* **9** (2018).
19. A. Maresca, M. Zaffagnini, L. Caporali, V. Carelli, C. Zanna, DNA methyltransferase 1 mutations and mitochondrial pathology: is mtDNA methylated? *Front Genet* **6**, 90 (2015).
20. A. Scott, J. Song, R. Ewing, Z. Wang, Regulation of protein stability of DNA methyltransferase 1 by post-translational modifications. *Acta Biochim Biophys Sin (Shanghai)* **46**, 199-203 (2014).
21. R. Lister *et al.*, Human DNA methylomes at base resolution show widespread epigenomic differences. *Nature* **462**, 315-322 (2009).
22. B. P. Berman *et al.*, Regions of focal DNA hypermethylation and long-range hypomethylation in colorectal cancer coincide with nuclear lamina-associated domains. *Nat Genet* **44**, 40-46 (2011).
23. A. B. Brinkman *et al.*, Partially methylated domains are hypervariable in breast cancer and fuel widespread CpG island hypermethylation. *Nat Commun* **10**, 1749 (2019).
24. R. S. Hansen *et al.*, Sequencing newly replicated DNA reveals widespread plasticity in human replication timing. *Proc Natl Acad Sci U S A* **107**, 139-144 (2010).
25. W. Zhou *et al.*, DNA methylation loss in late-replicating domains is linked to mitotic cell division. *Nat Genet* **50**, 591-602 (2018).
26. B. E. Decato *et al.*, Characterization of universal features of partially methylated domains across tissues and species. *Epigenetics Chromatin* **13**, 39 (2020).
27. S. E. S. Martin *et al.*, Structure-Based Evolution of Low Nanomolar O-GlcNAc Transferase Inhibitors. *J Am Chem Soc* **140**, 13542-13545 (2018).
28. A. A. Elbatrawy, E. J. Kim, G. Nam, O-GlcNAcase: Emerging Mechanism, Substrate Recognition and Small-Molecule Inhibitors. *ChemMedChem* **15**, 1244-1257 (2020).
29. S. R. Andrews *et al.*, Substrate specificity in glycoside hydrolase family 10. Tyrosine 87 and leucine 314 play a pivotal role in discriminating between glucose and xylose binding in the proximal active site of Pseudomonas cellulosa xylanase 10A. *J Biol Chem* **275**, 23027-23033 (2000).
30. H. J. Kao *et al.*, A two-layered machine learning method to identify protein O-GlcNAcylation sites with O-GlcNAc transferase substrate motifs. *BMC Bioinformatics* **16 Suppl 18**, S10 (2015).
31. C. Yompakdee *et al.*, A putative new membrane protein, Pho86p, in the inorganic phosphate uptake system of Saccharomyces cerevisiae. *Gene* **171**, 41-47 (1996).
32. O. Yarychkivska, Z. Shahabuddin, N. Comfort, M. Boulard, T. H. Bestor, BAH domains and a histone-like motif in DNA methyltransferase 1 (DNMT1) regulate de novo and maintenance methylation in vivo. *The Journal of biological chemistry* **293**, 19466-19475 (2018).

33. H. Zhou *et al.*, Toward a comprehensive characterization of a human cancer cell phosphoproteome. *Journal of proteome research* **12**, 260-271 (2013).
34. X. Li, Y. Liu, T. Salz, K. D. Hansen, A. Feinberg, Whole-genome analysis of the methylome and hydroxymethylome in normal and malignant lung and liver. *Genome Res* **26**, 1730-1741 (2016).
35. C. Chang *et al.*, Systematic analyses of the transcriptome, translatome, and proteome provide a global view and potential strategy for the C-HPP. *J Proteome Res* **13**, 38-49 (2014).
36. R. E. Thurman, N. Day, W. S. Noble, J. A. Stamatoyannopoulos, Identification of higher-order functional domains in the human ENCODE regions. *Genome Res* **17**, 917-927 (2007).
37. J. R. Edwards, O. Yarychkivska, M. Boulard, T. H. Bestor, DNA methylation and DNA methyltransferases. *Epigenetics Chromatin* **10**, 23 (2017).
38. W. Zhou, G. Liang, P. L. Molloy, P. A. Jones, DNA methylation enables transposable element-driven genome expansion. *Proc Natl Acad Sci U S A* **117**, 19359-19366 (2020).
39. M. V. Almeida, G. Vernaz, A. L. K. Putman, E. A. Miska, Taming transposable elements in vertebrates: from epigenetic silencing to domestication. *Trends Genet* 10.1016/j.tig.2022.02.009 (2022).
40. S. Brimble, E. E. Wollaston-Hayden, C. F. Teo, A. C. Morris, L. Wells, The Role of the O-GlcNAc Modification in Regulating Eukaryotic Gene Expression. *Curr Signal Transduct Ther* **5**, 12-24 (2010).
41. C. Ling, T. Ronn, Epigenetics in Human Obesity and Type 2 Diabetes. *Cell Metab* **29**, 1028-1044 (2019).
42. A. Vasconcelos-Dos-Santos, R. M. de Queiroz, B. da Costa Rodrigues, A. R. Todeschini, W. B. Dias, Hyperglycemia and aberrant O-GlcNAcylation: contributions to tumor progression. *J Bioenerg Biomembr* **50**, 175-187 (2018).
43. C. Bauer *et al.*, Phosphorylation of TET proteins is regulated via O-GlcNAcylation by the O-linked N-acetylglucosamine transferase (OGT). *The Journal of biological chemistry* **290**, 4801-4812 (2015).
44. J. P. Etchegaray, R. Mostoslavsky, Interplay between Metabolism and Epigenetics: A Nuclear Adaptation to Environmental Changes. *Molecular cell* **62**, 695-711 (2016).
45. Y. Yang *et al.*, O-GlcNAc transferase inhibits visceral fat lipolysis and promotes diet-induced obesity. *Nat Commun* **11**, 181 (2020).
46. H. Li, Minimap2: pairwise alignment for nucleotide sequences. *Bioinformatics* **34**, 3094-3100 (2018).
47. N. J. Loman, J. Quick, J. T. Simpson, A complete bacterial genome assembled de novo using only nanopore sequencing data. *Nat Methods* **12**, 733-735 (2015).

Figures

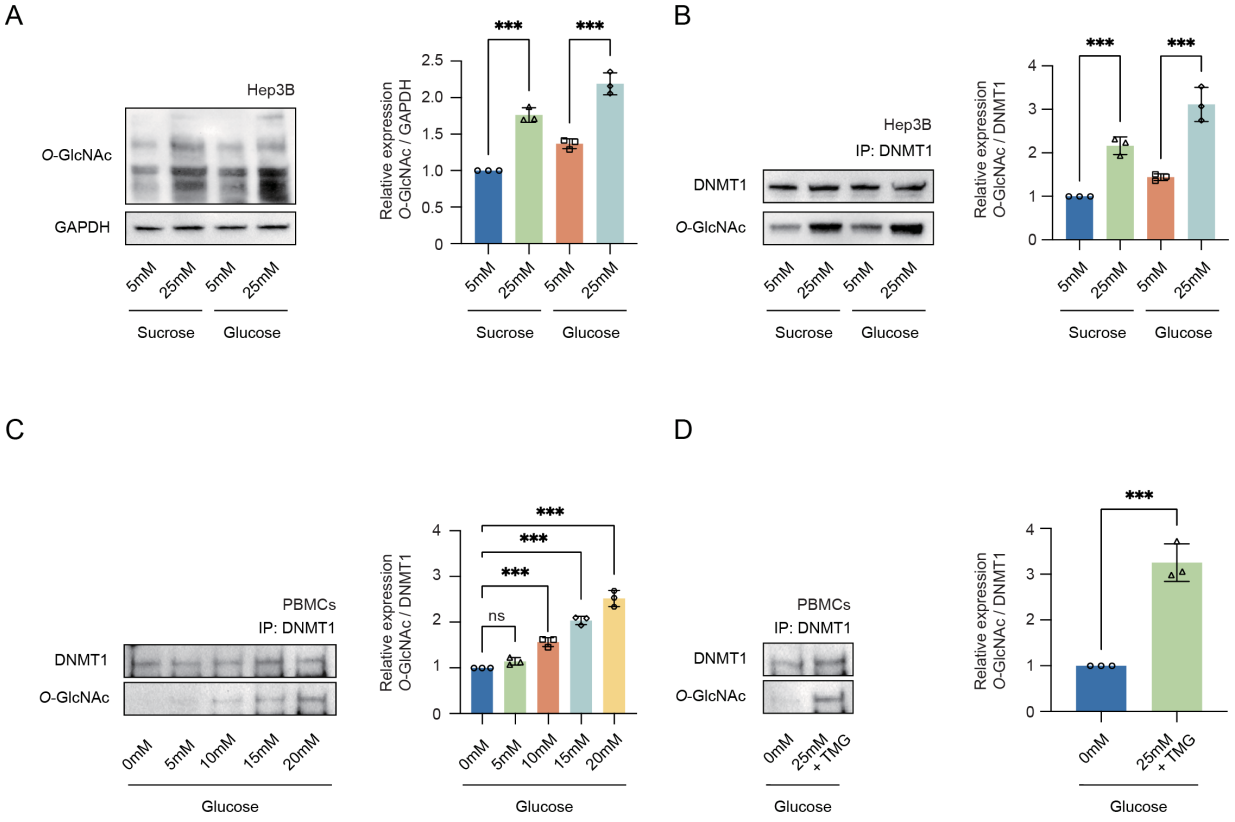

Fig. 1. High glucose increases *O*-GlcNAcylation of DNMT1 in cell lines and primary cells. (*A*) Hep3B cells were treated glucose or sucrose (5mM or 25mM). Shown are immunoblots of collected lysates using antibody targeting *O*-GlcNAc and GAPDH (n = 3). (*B*) Lysates of Hep3B treated with glucose were immunoprecipitated with DNMT1 and immunoprecipitates were immunoblotted with antibody targeting *O*-GlcNAc (n = 3). (*C*) PBMCs were isolated from three individual donor blood samples and treated with increasing concentration of glucose for 24 hours. Collected cell lysates from PBMCs were immunoprecipitated with antibody targeting DNMT1 and immunoblotted for *O*-GlcNAc. This is from one donor set. (n = 3). (*D*) Pooled PBMCs treated with 25 mM glucose with Thiamet-G were immunoprecipitated with antibody targeting DNMT1 and immunoblotted for *O*-GlcNAc (n = 3). ***$p < 0.0001$ by Student's *t*-test (*A*-*D*); n.s., not significant; Data are represented as mean ± SD from three replicates of each sample.

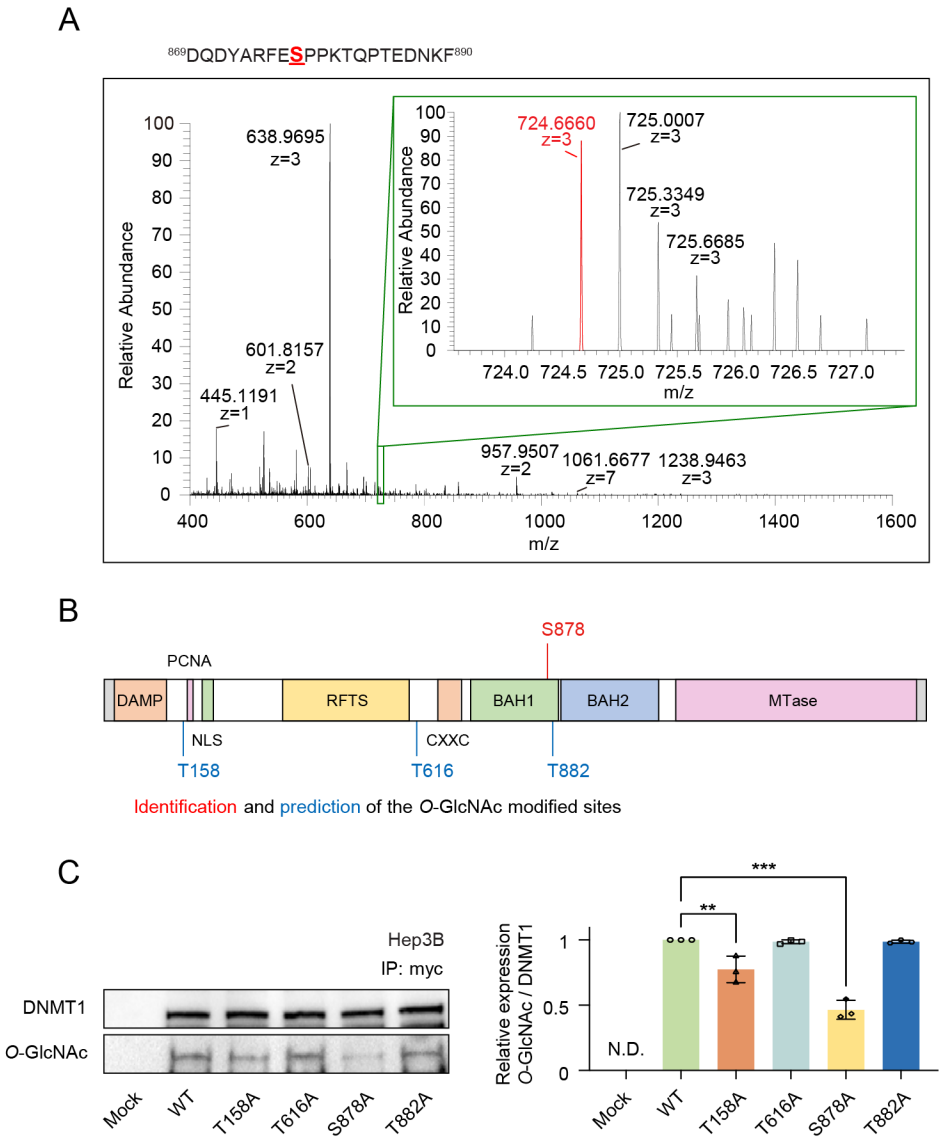

Fig. 2. Identification of *O*-GlcNAcylated sites within DNMT1 by LC-MS/MS. (*A*) Schematic drawing of the DNMT1 *O*-GlcNAc modified region enriched from Hep3B cells based on mass spectrometry (MS) data and tandem MS (MS/MS) peaks. FTMS + p NSI Full MS [400.0000-1600.0000]. DQDYARFESPPKTQPTEDNKF (S9 HexNAc) – S878. (*B*) Schematic diagram of identified novel *O*-GlcNAcylated sites within DNMT1 as determined via MS and OGTsite. DMAP, DNA methyltransferase associated protein-binding domain; PCNA, proliferating cell nuclear antigen-binding domain; NLS, nuclear localization sequences; RFTS, replication foci targeting sequence domain; BAH, bromo-adjacent homology domain. (*C*) Each immunoprecipitated Myc-DNMT1 wild type and substituted mutants was immunoblotted with an *O*-GlcNAc antibody (n = 3).

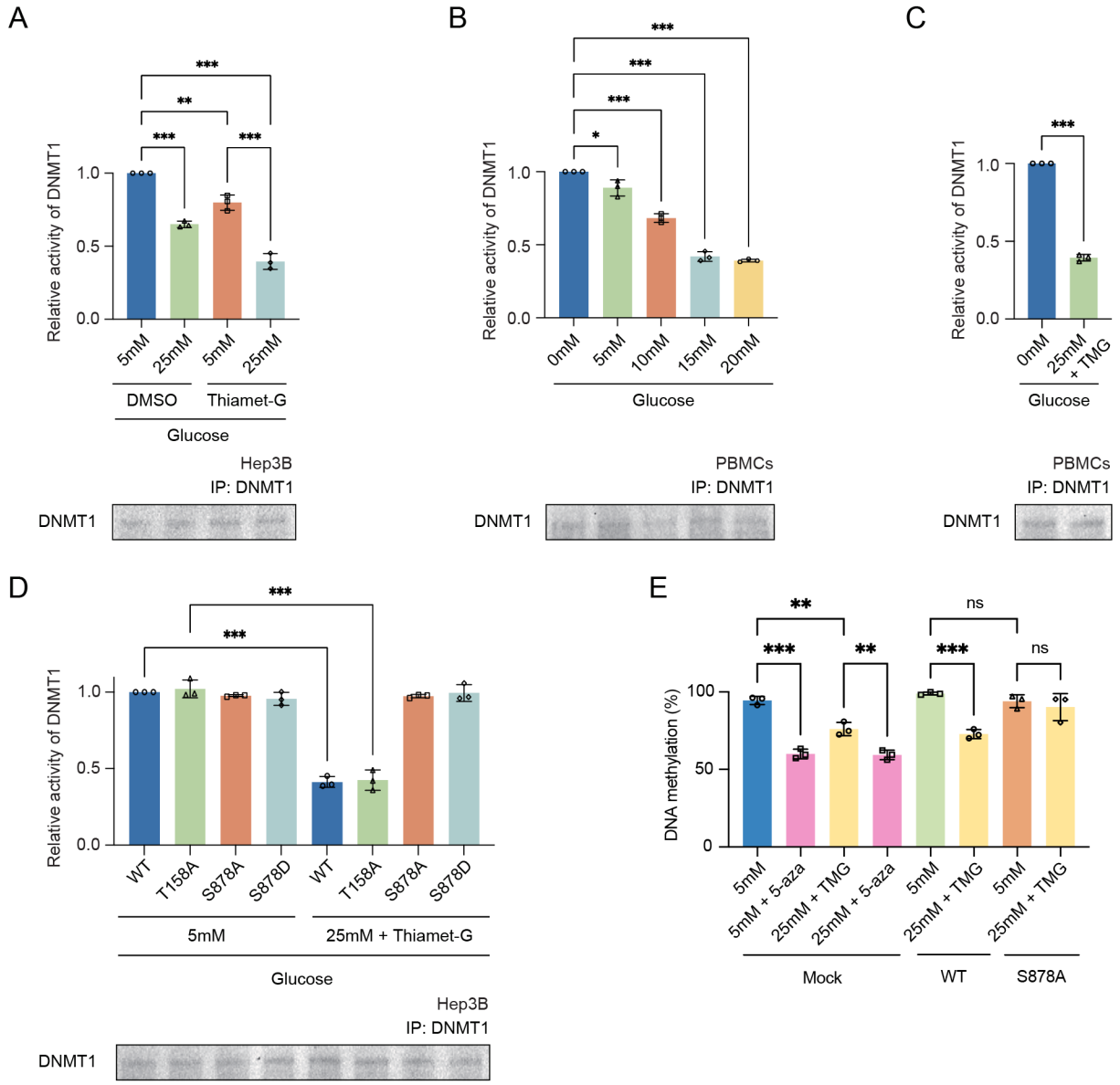

Fig. 3. Site specific *O*-GlcNAcylation inhibits DNMT1 methyltransferase function. For (*A*)-(*D*), bar graphs are of relative activity of DNA methyltransferase activity measured as absorbance from of DNMT Activity/Inhibition ELISA easy kit and representative immunoblots of immunoprecipitates performed with antibodies targeting DNMT1. (*A*) Hep3B cells were treated 5mM or 25mM glucose with or without TMG (n = 3). (*B*) PBMCs from donors were treated with increasing concentrations of glucose (range: 0-20mM) (n = 3). (*C*) PBMCs from donors were treated 5mM or 25mM glucose with TMG (n = 3). (*D*) Each immunoprecipitated Myc-DNMT1 wild type and substituted mutants were treated with 5mM or 25mM glucose (n = 3). (*E*) Each Hep3B and Myc-DNMT1 overexpressed mutants (DNMT1-WT or DNMT1-S878A) were treated 5mM or 25mM glucose or 5-aza (negative control). Shown are absorbance of global DNA methylation of LINE-1 performed with global DNA methylation LINE-1 kit. (n = 3). *$p < 0.001$; **$p < 0.005$; ***$p < 0.0001$ by Student's *t*-test (*A*-*E*); ns, not significant; Data are represented as mean ± SD from three replicates of each sample.

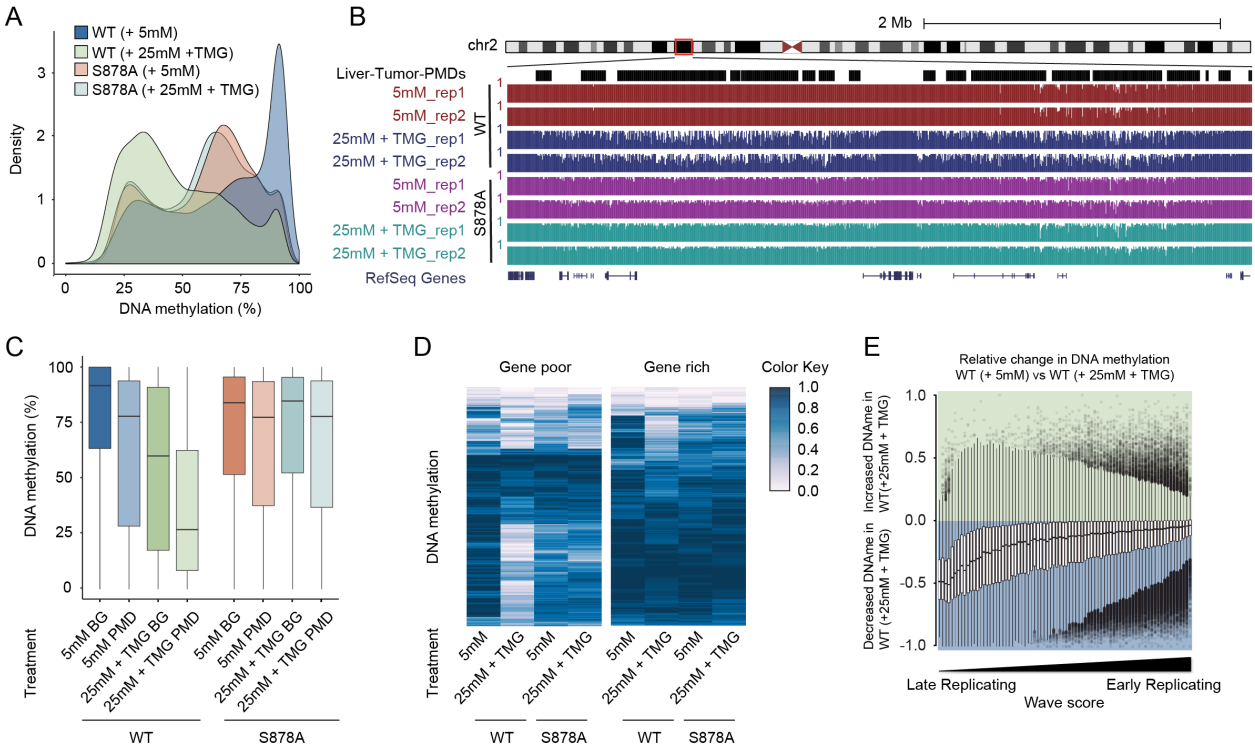

Fig. 4. High glucose leads to loss of DNA methylation at cancer specific partially methylated domains (PMDs). (*A*) Density plot of DNA methylation for DNMT1-WT and DNMT1-S878A cells and low or high glucose. (*B*) Genome browser screenshot of DNA methylation for DNMT1-WT and DNMT1-S878A cells and low or high glucose along with liver tumor PMDs from (34). (*C*) Boxplots of DNA methylation at PMDs or general genomic background (BG) for each DNMT1-WT and DNMT1-S878A treated with low or high glucose. (*D*) Heatmap representation of global DNA methylation for DNMT1-WT and DNMT1-S878A cells under low or high glucose at gene poor and gene rich regions. (*E*) Methylation changes from *O*-GlcNAcylation of DNMT1 by wave score for replication timing (24, 36).